Targeting cancer cells and tumor microenvironment in preclinical and clinical models of Hodgkin lymphoma using the dual PI3Kδ/γ inhibitor RP6530

Silvia L. Locatelli,[1] Giuseppa Careddu,[1] Simone Serio,[1] Francesca M. Consonni,[2] Akihiro Maeda,[2] Srikant Viswanadha,[3] Swaroop Vakkalanka,[4] Luca Castagna,[1] Armando Santoro,[1,5] Paola Allavena,[2,5] Antonio Sica,[2,6] Carmelo Carlo-Stella[1,5]

[1]Department of Oncology and Hematology, Humanitas Cancer Center, Humanitas Clinical and Research Center, Rozzano, Milan, Italy.
[2]Department of Inflammation and Immunology, Humanitas Clinical and Research Center, Rozzano, Milan, Italy.
[3]Incozen Therapeutics, Hyderabad, India.
[4]Rhizen Pharmaceuticals S A, La Chaux-de-Fonds, Switzerland.
[5]Department of Biomedical Sciences, Humanitas University, Rozzano, Milan, Italy.
[6]Department of Pharmaceutical Sciences, Università del Piemonte Orientale "Amedeo Avogadro", Novara, Italy.

Running title: PI3Kδ/γ inhibition targets HL TME and cancer cells

Keywords: PI3Kδ/γ inhibitor, Hodgkin lymphoma, tumor-associated macrophages, macrophage repolarization, tumor angiogenesis

Financial support: This work was supported in part by grants from the Italian Association for Cancer Research, Milan, Italy (AIRC, project no. 16722 to C.C.-S); Fondazione Regionale Ricerca Biomedica, Milan, Italy (FRRB project no. 2015-0042 to A.S.); Worldwide Cancer Research, UK (grant #15-1346 to P. A.); Ministero dell'Istruzione dell'Università e della Ricerca (MIUR), Milan, Italy (PRIN, project no. C52F16000940001 to A. Sica); Irish Research Council 2017, Ireland (IRC, project no. 19885 A. Sica). S.L.L. is supported by Fondazione Regionale Ricerca Biomedica, Milan, Italy (FRRB project no. 2015-0042). A.M. is recipient of a Marie Skłodowska-Curie Individual European Fellowship-H2020-MSCA-IF-2015-EF-ST (No.706557).

Corresponding authors: Carmelo Carlo-Stella, Department of Oncology and Hematology, Humanitas Cancer Center, Humanitas Clinical and Research Center and Department of Biomedical Sciences, Humanitas University, Via Manzoni 56, 20089 Rozzano, Milan, Italy**.** Phone: +39 02 8224 4577; Fax: +39 02 8224 4590; E-mail: carmelo.carlostella@hunimed.eu; and Silvia Laura Locatelli, Ph.D., Department of Oncology and Hematology, Humanitas Cancer Center, Via Manzoni 113, 20089 Rozzano, Milan, Italy. Phone: +39 02 8224 5253; Fax: +39 02 8224 5191; E-mail: silvia.locatelli@cancercenter.humanitas.it.

Conflict of interest disclosure: S. Viswanadha (Employment – Incozen Therapeutics), S. Vakkalanka (Equity & Employment – Rhizen Pharmaceuticals).

Word count: 4983
Total no. of figures/tables: 6/0

Statement of translational relevance

In preclinical and clinical models of Hodgkin lymphoma (HL), the PI3Kδ/γ inhibitor RP6530 exerts a direct cytotoxic effect on HL cells and reprogrammes the tumor-associated macrophages (TAMs) from a protumor M2 phenotype to an antitumor M1 phenotype, thus reshaping the interplay between cancer cells and their tumor microenvironment (TME). As a consequence of TME reprogramming induced by the PI3Kδ/γ inhibition, HL tumor cells as well as tumor vasculature are effectively reduced. Our data establish the first evidence of the translational potential of PI3Kδ/γ inhibition in suppressing malignant cell growth and reshaping the microenvironment of HL, suggesting that a novel unique therapeutic opportunity may be achievable for treatment of HL patients.

Abstract

Purpose: Tumor-associated macrophages (TAMs) and the hyperactivation of phosphoinositide 3-kinase (PI3K)/AKT pathway are involved in the pathogenesis of Hodgkin lymphoma (HL) and affect disease outcome. Since the δ and γ isoforms of PI3K are overexpressed in Hodgkin/Reed-Sternberg (HRS) cells and the tumor microenvironment (TME), we propose that the PI3Kδ/γ inhibitor RP6530 might affect both HRS cells and TME, ultimately leading to an enhanced antitumor response.

Experimental design: HL cell lines (L-540, KM-H2 and L-428) and primary human macrophages were used to investigate the activity of RP6530 *in vitro* and *in vivo* in HL cell line xenografts.

Results: *In vitro*, RP6530 besides killing and inhibiting the proliferation of HL cells, downregulated lactic acid metabolism, switching the activation of macrophages from an immunosuppressive M2-like phenotype to a more inflammatory M1-like state. By RNA sequencing, we define tumor glycolysis as a specific PI3Kδ/γ-dependent pathway implicated in the metabolic reprogramming of cancer cells. We identify the metabolic regulator Pyruvate Kinase M2 (PKM2) as the main mediator of tumor-induced immunosuppressive phenotype of macrophages. Furthermore, we show in human tumor xenografts that RP6530 repolarizes TAMs into pro-inflammatory macrophages and inhibits tumor vasculature, leading to tumor regression. Interestingly, HL patients experiencing objective responses (CR and PR) in a phase 1 trial using RP6530 showed a significant inhibition of circulating MDSCs and an average mean reduction in serum TARC levels of 40% (range, 4–76%).

Conclusions: Our results support PI3Kδ/γ inhibition as a novel therapeutic strategy that targets both malignant cells and the TME to treat HL patients.

Introduction

Primary refractory and early-relapsed Hodgkin lymphoma (HL) patients experience poor responses to salvage chemotherapy and dismal long-term disease control (1-3). Despite the variety of novel therapeutic options, they represent an unmet medical need urgently requiring novel therapeutic agents to overcome the chemo-refractory phenotype (4-8).

The phosphoinositide 3-kinase (PI3K)/Akt pathway is implicated in the pathogenesis of HL (9). The δ isoform of PI3K is highly expressed in tissues of hematopoietic origin and is involved in the activation, proliferation, survival, homing and retention of B-cells in lymphoid tissues (10). Idelalisib is the first PI3Kδ inhibitor to be approved for follicular lymphoma and chronic lymphocytic leukemia (11, 12), and we previously reported that PI3Kδ isoform inhibition results in direct HL cell killing (13). The PI3Kγ isoform, although highly expressed in leukocytes, may play a more crucial role in the immune system than that in oncogenesis (10). To date, much effort has been devoted to PI3Kγ as a target in inflammatory diseases driven by leukocytes (14). Inflammation driven by Tumor-associated macrophages (TAMs) is now considered a hallmark of cancer, contributing to both cancer cell expansion and angiogenesis (15). Recent data in solid tumors show that selectively targeting the γ isoform of PI3K in TAMs modulates the immunosuppressive tumor microenvironment (TME), resulting in tumor regression (16-18).

TAMs have been implicated in the pathogenesis of HL and have been suggested to negatively impact clinical outcome (19-23). Both the δ and γ isoforms of PI3K are overexpressed in HRS cells and cell of the microenvironment, respectively, thereby representing attractive therapeutic targets (24). Here, we describe the effects of RP6530, a novel PI3Kδ/γ inhibitor currently in phase I-II clinical trials in Europe and the United States. RP6530 exhibits high anti-proliferative and cytotoxic activity in HL cell lines *in vitro* and potent efficacy *in vivo* in preclinical xenograft mouse models. We show that RP6530 downregulates lactic acid metabolism in HL cells, reducing M2-like polarization of macrophages. Furthermore, we demonstrate that this effect is mediated by the metabolic regulator pyruvate kinase M2 (PKM2). RP6530 reshapes the TME, inhibits angiogenesis, and switches TAM activation from an immunosuppressive M2-like phenotype to a more inflammatory M1-like state. We propose that dual pharmacological targeting of the δ and γ

PI3K isoforms affects both malignant tumor cells and the TME, ultimately leading to an enhanced antitumor response. The ability of RP6530 to affect both HL tumor cells and the HL TME indicates that a novel unique therapeutic opportunity may be achievable for treatment of HL patients.

Materials and Methods

Reagents. Rhizen Pharmaceuticals, SA (La Chaux-de-Fonds, Switzerland) kindly provided the PI3Kδ/γ inhibitor RP6530. RP6530 had high potency against PI3Kδ (IC_{50} = 24.5 nM) and γ (IC_{50} = 33.2 nM) enzymes with selectivity over α (> 300-fold) and β (> 120-fold) isoforms with specificity being similar in isoform-specific cell-based assays as well (25). For *in vitro* experiments, RP6530 was reconstituted in 100% DMSO and further diluted in RPMI-1640 to final concentrations of 0.05% and 0.1% DMSO (v/v). For *in vivo* experiments, RP6530 was dissolved in 0.5% methylcellulose (pH 2.2).

Cell death and cell proliferation assay. HL cell lines (4 x 10^5 ml^{-1}) were cultured in the absence or presence of RP6530 (ranging between 1.25 and 10 µM) for 24, 48 and 72 h. Dead and proliferating cells were detected by annexin-V/propidium iodide double staining (Immunostep) and WST assay (BioVision), respectively, according to the manufacturer's instructions. See Supplements for further information.

Cell cycle analysis. HL cell lines were cultured in the absence or presence of RP6530 (5 or 10 µM) for 48 h, fixed in 70% ethanol, and then stained with 2.5 µg ml^{-1} PI (Calbiochem). Cell cycle status was measured using a FACSCalibur flow cytometry system (BD Biosciences) and analyzed using FlowJo software (Treestar).

RNA preparation and sequencing. polyA-RNA-seq was performed on HL cell lines (L-540 and KM-H2) after RP6530 100 nM for 6 h and after RP6530 10 µM for 6 and 24 h. Two biological replicates were profiled for each experimental condition. RNA was purified using an RNeasy Mini Kit (Qiagen) and treated with DNase according to the manufacturer's protocol. Total RNA quality was evaluated using an Agilent Bioanalyzer and an RNA Nano kit. Only samples with an RIN score ≥ 8 were processed further. RNA-seq libraries were sequenced using a TruSeq stranded mRNA kit (Illumina) according to the manufacturer's instructions. See Supplements for further information.

RNA-Seq analysis. RNA-Seq samples were demultiplexed, and FASTQ files were created from BCL files using bcl2fastq (Illumina). Quality control and assessment were performed using FastQC v0.11 (http://www.bioinformatics.babraham.ac.uk/projects/fastqc). STAR v2

was used to align each sample's single-end reads to the Gencode Human reference genome (build GRCh38). The raw read counts were normalized with TMM using edgeR package in R/Bioconductor. Differentially expressed transcripts were calculated in RPKM using edgeR. Significant genes were selected based on an FDR ≤ 0.1 and logCPM ≥ 0.5. Hierarchical clustering of the log2 fold change (log2FC) between the vehicle and RP6530-treated samples at 6 and 24 h was performed with cluster 3.0 using the complete linkage method and visualized using Java TreeView (NCBI Gene Express Omnibus website, GSE105439).

Pathway analysis. Pathway analysis was performed using QIAGEN's commercial Ingenuity Pathway Analysis (IPA, www.qiagen.com/ingenuity) software. GSEA was used in pre-ranked mode. The rank metric was calculated as the sign of log2FCs multiplied by the inverse of adjusted p-values. The gene sets used for this analysis were the C2:CP:KEGG and C2:CP:PID Curated Molecular Signatures Database (MSigDB) gene sets. Enrichr was used to find significantly enriched (adjusted p-value ≤ 0.1) KEGG and PID terms for the gene set continuously modulated during the time course. PPI networks for the select MSigDB gene set pathways (KEGG_GLYCOLYSIS_GLUCONEOGENESIS and PID_HIF1_TFPATHWAY) were constructed using the STRING database (http://www.string-db.org/). See Supplements for further information.

Human macrophage differentiation and culture. Human leukocytes from apheresis blood products were obtained from the Pavia Blood Bank. Cells were diluted in PBS and centrifuged over Histopaque 1077 to purify mononuclear cells. An EasySep Human Monocyte Enrichment Kit (Stemcell Technologies) was used to isolate monocytes from peripheral blood mononuclear cells by negative selection. Purified monocytes were cultured in RPMI supplemented with 10% FBS and 50 ng ml^{-1} human mCSF (PeproTech). Non-adherent cells were removed after 2 h by washing, and adherent cells were cultured for 6 days to fully differentiate macrophages.

Macrophage polarization assay. Peripheral blood-derived macrophages were polarized toward an M1 phenotype with the addition of IFNγ (20 ng ml^{-1}, Peprotech) and LPS (100 ng ml^{-1}, Alexis) or toward an M2 phenotype with the addition of IL4 (20 ng ml^{-1}, Peprotech) for 24 h. Polarized macrophages were incubated with RP6530 (10 μM) for 24 h, and mRNA

178 expression and flow cytofluorimetric analyses were then performed. RNA was harvested
179 from the cells (Qiagen RNeasy), and SYBR green-based qPCR was performed using primers
180 for human *CXCL9, IL12p40, CXCL11, CXCL10, CD80, CCL17, CCL22, IL10, CD301,* and *CD163.*
181 mRNA levels were normalized to *actin* expression ($\Delta C_t = C_t^{\text{gene of interest}} - C_t^{Actin}$) and
182 reported as relative mRNA expression ($\Delta\Delta Ct = 2^{-(\Delta Ctsample - \Delta Ctcontrol)}$). Primary antibodies to cell
183 surface markers directed against CD14 (M5E2) and CD80 (L307) were from BD Pharmingen,
184 and primary antibodies to cell surface markers directed against CD40 (HB14), CD209
185 (9E9A8), and CD301 (H037G3) were from eBioscience.
186
187 **siRNA-mediated gene silencing.** HL cell lines (3×10^5) were transfected using Lipofectamine
188 RNAiMAX transfection reagent (Thermo Fisher Scientific) with 1 nmol PKM2 siRNA (#285
189 and #286) or Silencer Select Negative Control siRNA (#AM4621 and #AM4611) (Thermo
190 Fisher Scientific) for 48 h according to the manufacturer's instructions.
191
192 **Transwell co-culture assay.** HL cells (3×10^5 cells) were plated in the lower compartment of
193 6.5-mm polycarbonate Transwell inserts (pore size 0.4 µm; Corning) and exposed to RP6530
194 (10 µM) or siRNA transfection as described in the previous section. The next day, $3 \times$
195 10^5 M2-polarized macrophages were placed in the upper compartment of the Transwell
196 inserts and co-cultured with the HL cells. After 24-48 h of co-culture, RNA was extracted
197 from the macrophages in the upper inserts, and HL cells were washed and then used for
198 subsequent experiments. Control wells contained either HL cells only in the lower
199 compartment with RPMI in the upper compartment or RPMI in the lower compartment with
200 only M2-polarized macrophages or M0 macrophages in the upper compartment.
201
202 **Immunoblotting.** HL cell lines or polarized M1 and M2 macrophages were treated with
203 RP6530 as described in the figure legends and proteins were detected with the indicated
204 antibodies. See Supplements for further information.
205
206 **Biochemical assays.** The lactate concentration in HL cell and polarized macrophage lysates
207 was measured after RP6530 (10 µM) treatment with an L-Lactate Assay Kit (Abcam)
208 according to the manufacturer's instructions.
209

Enzyme-linked immunosorbent assay. Serum samples were centrifuged at 4,000 rpm for 10 minutes and then kept at -80 °C until enzyme-linked immunosorbent assay (ELISA) assessment. Serum levels of TARC/CCL17 were determined according to the manufacturer's instructions (R&D Systems). The TARC/CCL17 level in patient sera samples was determined by correlating each value duplicate with a standard curve based on a 2-fold serial dilution of recombinant TARC/CCL17 with known concentration.

Flow cytometry staining and analysis. Single-cell suspensions (10^6 cells in 100 µl total volume) were incubated with FcR-blocking reagent (BD Biosciences) at 4 °C for 30 min. Staining of cell surface markers was performed at 4 °C for 20 min with the following primary antibodies: anti-mouse F4/80 (BM8), anti-mouse CD45 (30-F11), anti-mouse/human CD11b (M1/70), anti-mouse CD86 (GL-1), anti-mouse CD301 (LOM-14), anti-mouse MHC-II (M5/114.15.2), anti-mouse CD206 (C068C2), anti-mouse Ki-67 (16A8), anti-human HLA-DR (L243), anti-human CD14 (M5E2) anti-human CD33 (WM53) (Biolegend); and anti-mouse Ly6G (1A8) and anti-mouse Ly6C (HK1.4) (eBioscence). Unconjugated rabbit anti-mouse NOS2 (Abcam) was also used followed by incubation with secondary goat anti-rabbit Alexa Fluor 647-conjugated antibody (Invitrogen, Molecular Probes, Carlsbad, CA). For the gating of the viable cells, a LIVE/DEAD™ Fixable Violet Dead Cell Stain Kit (Thermo Fisher) was used. For intracellular staining, a Cytofix/Cytoperm and Permwash staining kit (BD Pharmigen) was used according to the manufacturer's instructions. Multicolor FACS analysis was performed on a BD FACSCanto II flow cytometer. All data analysis was performed using the flow cytometry analysis program FlowJo (Treestar).

Tumor challenge and treatment experiments. Six- to eight-week-old NOD/SCID mice (20 to 25 g) were purchased from Charles River Labs and xenografted with L-540 (25×10^6 cells) and KM-H2 (20×10^6 cells) cells by subcutaneous inoculation into the right flank. The treatments started when the tumors were palpable (approximately 200 mm^3). RP6530 was administered by oral gavage twice per day at 100 and 150 mg kg^{-1} for 3 weeks or at 150 mg kg^{-1} for 5 days. The control groups received a vehicle (0.5% methylcellulose, pH 2.2) without the active product. When appropriate, *in vivo* biotinylation of tumor vasculature (26) was performed 5 days after RP6530 treatment and 3 h after the last drug administration. The animal experiments were performed according to EU 86/109 Directive (D.L. 116/92 and

following additions) and were approved by the institutional Ethical Committee for Animal Experimentation of the Humanitas Clinical and Research Center. See Supplements for further information.

Tumor-infiltrating myeloid cell analysis. Six- to eight-week-old NOD/SCID mice were injected subcutaneously with L-540 (25×10^6 cells) and KM-H2 (20×10^6 cells) cells in 400 µl of PBS in the right flank. On days 19 (for L-540) or 25 (for KM-H2) after tumor injection, the tumor-bearing mice were grouped and treated with RP6530 (150 mg kg^{-1}, twice per day, orally) or vehicle (0.5% methylcellulose, pH 2.2) for 5 days. Three hours after the final treatment, the mice were euthanized, and the tumors were snap frozen or digested in a mixture of 0.5 mg ml^{-1} collagenase IV and 150 U ml^{-1} DNase I in RPMI-1640 for 30 min at 37 °C. Tumor-infiltrating myeloid cells were analyzed by immunohistochemistry and flow cytometry. Tumor macrophage enrichment was performed by plating cells in FBS-free RPMI containing 1% penicillin/streptomycin for 1 h at 37 °C and 5% CO_2. After 1 h, non-adherent cells were removed with three PBS washes, and RNA was harvested from tumor macrophages (Qiagen RNeasy). SYBR green-based qPCR was performed using primers for murine *IL1β, CXCL10, iNOS, TNFα, CD80, CXCL11, IL6, Arg1, CCL22, CCL2, IL10, CD163, CD206, TGFβ, PGF, IGF1, EGF, FGF2, VEGFA, HIF-1α,* and *PD-L1* (Sigma-Aldrich). mRNA levels were normalized to actin levels ($\Delta Ct = Ct^{\text{gene of interest}} - Ct^{\text{Actin}}$) and reported as a fold change in the RP6530-treated mice over the vehicle-treated controls.

Immunofluorescence. The *in vivo* biotinylated tumor nodules were incubated with incubated with Alexa568-streptavidin (Invitrogen), pAKT (Ser473) (736E11), pERK1/2 (197G2), and caspase-3 (E-8) antibodies (Santa Cruz), PKM2 (D78A4) from Cell Signaling Technology, CD163 (EPR19518) from Novus Biologicals, MHC-II (OX-6) from Abcam and F4/80 (CI:A3-1) from Bio-Rad. See Supplements for further information.

Immunohistochemistry. Sections from FFPE lymph node biopsies obtained from consenting patients at the time of diagnostic workup or HL cell line cytospins were stained with the following antibodies: p110δ (EPR986) from Novus Biologicals; p110γ (#PA5-28070) from Thermo Fisher Scientific; and pAkt (S473) (736E11), pAkt (T308) (L32A4), pS6 (#2211), and pERK1/2 (20G11) from Cell Signaling Technology. Cryostat sections of *in vivo* biotinylated

tumor nodules were stained with F4/80 (CI:A3-1) from Bio-Rad, HRP-conjugated streptavidin, Ki-67 (MIB-1) from Dako and VEGF (ab46154) from Abcam. Tumor apoptosis and necrosis were detected via TUNEL staining (Roche). See Supplements for further information.

Statistics. Analysis for significance was performed using one-way ANOVA with a Tukey's post hoc test for multiple pairwise testing of more than two groups and by parametric Student's t-test when only two groups were compared. Two-way ANOVA with Tukey's post hoc test and Dunnett's post hoc test was performed when comparing more than two groups and two variables.

Results

RP6530 inhibits the PI3K/AKT and ERK signaling pathways in HL cells. The PI3K/Akt pathway is consistently activated in HL (24). The δ and γ isoforms of PI3K are highly expressed both in primary HRS cells and microenvironmental cells (**Supplementary Fig. S1A**). The multiple roles of PI3Kδ and PI3Kγ in HRS cells and reactive cells of the microenvironment support the hypothesis that blocking δ and γ isoforms may provide a therapeutic benefit. To investigate these hypothesis, HL cell lines (L-540, KM-H2 and L-428) displaying an expression pattern of PI3K δ and γ isoforms similar to that of primary HRS cells were used to assess the effects of the PI3Kδ/γ dual inhibitor RP6530 (**Supplementary Fig. S1B**). Based on pharmacokinetic studies performed in patients enrolled in phase 1 trial (clinicaltrials.gov identifier NCT02017613) using RP6530, drug concentrations up to 10 µM are pharmacologically achievable (*C. Carlo-Stella et al., manuscript in preparation*). Exposure of HL cell lines to RP6530 (1.25 µM to 10 µM) led to a dose-dependent inhibition of phosphorylation of ERK1/2, Akt and its downstream target proteins (**Fig. 1A-C**), indicating that targeting PI3Kδ/γ affects both the Akt and MAPK pathways.

RP6530 inhibits cell proliferation through induction of G0/G1 arrest and apoptosis. Incubating L-540, KM-H2 and L-428 cell lines for up to 72 h with RP6530 (1.25 - 10 µM) resulted in a significant dose- and time-dependent decrease in cell proliferation down to 30% (**Fig. 1D**). The cell cycle data showed that treatment with RP6530 induced 2-fold accumulation of cells in the G0/G1 phase with an accompanying 4-fold decrease in cells in the S phase compared with vehicle controls (**Fig. 1E**). Additionally, caspase-dependent cell death was increased (up to 50%) after RP6530 treatment (**Fig. 1F-H**). These results showed that RP6530 inhibits cell proliferation through induction of G0/G1 arrest and apoptosis in HL cell lines.

Functional characterization of differentially expressed genes in RP6530-treated HL cell lines. Next, we evaluated by RNA-Seq the anti-lymphoma functions and the underlying genes affected by dual PI3Kδ/γ inhibition. Concordantly downregulated genes in L-540 and KM-H2 cells at 6 or 24 h time points were involved in cell proliferation, MAPK, JAK/STAT, IL2, IL4/STAT5, glycolysis, HIF1α and MYC signaling, whereas concordantly upregulated genes were involved in cell death, apoptosis and cell cycle deregulation (**Supplementary Fig. S2A-**

D; S3 and S4). We confirmed these findings with a much lower concentration of RP6530 (100 nM), which reduced the extent of off-target effects. (**Supplementary Fig. S5A**). A common gene expression signature was created consisting of genes consistently up- and downregulated across all time points in both cell lines (**Supplementary Fig. S2B and Fig. 2A**). Although no significantly enriched pathways were assessed in the 39 upregulated genes, the 111 genes downregulated following RP6530 treatment were highly enriched in tumor glycolysis and HIF1α signaling (**Fig. 2A**), a phenomenon already detectable at nM concentration of RP6530 (**Supplementary Fig. S5B-C**), supporting the strong relevance of those two pathways in the mechanism of action of RP6530. Among these genes, we identified 28 highly connected hub genes likely to be key drivers in both tumor glycolysis and HIF1α signaling (**Fig. 2B**). Pyruvate kinase muscle isozyme M2 (PKM2) was selected as the most important hub gene (**Fig. 2C; Supplementary Fig. S6A-B**). PKM2 catalyzes the final and rate-limiting reaction of the aerobic glycolysis, thus regulating lactic acid production (27) and the Warburg effect in cancer cells (28). Since lactic acid secreted by tumor cells also functions as a critical signaling factor for M2-like polarization of macrophages (28), we hypothesized that by downregulating PKM2, RP6530 might reduce M2 markers expression in M2 polarized macrophages (**Fig. 3A**). According to the decreased expression of PKM2 after RP6530 and PKM2 siRNA treatment (**Supplementary Fig. S6C**), we detected a 50% reduction in lactate levels in HL cell lines (**Fig. 3B**) and significant downregulation of the expression of the M2 markers *CCL17* and *CCL22* in the M2-like macrophage population (**Fig. 3C**), supporting an attenuation of the M2 phenotype. PKM2 therefore appears to be a critical determinant of the RP6530-mediated crosstalk between HL tumor cells and macrophages (**Fig. 3D**).

RP6530 repolarizes macrophages to an M1-like phenotype. Many studies have implicated the PI3K/Akt pathway in macrophage activation (29, 30). RP6530 reduced Akt phosphorylation (**Fig. 3E**) in primary human M1 or M2 stimulated macrophages (**Supplementary Fig. S7A**). Differential expression of PI3Kδ and PI3Kγ isoforms was observed in M1 or M2 macrophages; with abundant p110γ in both M1 and M2 macrophages, whereas low levels of p110δ in M1 macrophages compared with M2 macrophages (**Fig. 3E**). Indeed, M2 macrophages were more sensitive than M1 macrophages to RP6530-induced cell death

(**Supplementary Fig. S7B**) after 48 h, suggesting that the expression of the δ isoform of PI3K is a prerequisite for the cytotoxic activity of RP6530.

IRF/STAT signaling is crucial in modulating macrophage polarization. The activation of IRF/STAT pathway by Interferons (IFNs) induces an M1-like phenotype (via STAT1), while IL-4-induced IRF/STAT pathway activation generates an M2-like phenotype (via STAT6) (31). RP6530 sustained and activated STAT1 phosphorylation in M1 and M2 macrophages, respectively, while inhibiting STAT6 phosphorylation in M2 macrophages (**Fig. 3F**), suggesting that RP6530 directly regulates macrophage polarization. Consistent with these findings, RP6530 markedly inhibited PKM2 mRNA and protein expression (**Supplementary Fig. S8A-B**), leading to the inhibition of lactic acid production in both M1 and M2-like macrophages (**Supplementary Fig. S8C**). We further tested RNA and protein expression of M1 and M2 markers in M1 or M2 macrophages after RP6530 treatment. The expression of representative M2 markers (CCL17, CCL22, CD163) was reduced, while M1 markers (CXCL9, CXCL10, CXCL11) were higher in RP6530-treated M2 macrophages (**Fig. 3G and Supplementary Fig. S8D**). Taken together, these findings demonstrated that RP6530 switches the activation of macrophages from an immunosuppressive M2-like phenotype to an inflammatory M1-like state.

RP6530 induces functional reprogramming of TAMs and decreases MDSCs in preclinical models and clinical samples from a phase 1 study. Based on previously published data showing that PI3Kγ is predominantly expressed in the myeloid cell compartment (32), we reasoned that RP6530, as a dual PI3Kδ/γ inhibitor, might affect the accumulation of TAMs *in vivo* in HL tumors. Indeed, we showed a significant reduction of $F4/80^+$ TAMs in L-540 or KM-H2 tumors after RP6530 treatment ($P < 0.0001$) (**Fig. 4A-B**). Additionally, RP6530 skewed the macrophage phenotype toward classically activated macrophages (M1) *in vivo*. In RP6530-treated HL xenograft, a shift within the macrophage population towards fewer $CD206^+$ and $CD301^+$ macrophages (M2) and more $CD86^+$ and MHC-II^+ macrophages (M1) was detected (**Fig. 4C**). We further investigated whether RP6530 could influence the function of TAMs by directly modulating their activity, and indeed we observed a significant down-regulation of common M2-related genes such as arginase-1 (Arg1), IL-10, and CCL2, and a concomitant up-regulation of M1-related genes such as inducible nitric oxide synthase

(iNOS), CD80 and CXCL11 (**Fig. 4D and Supplementary Fig. S9**), resulting in a significantly increased M1:M2 ratio and in a less immunosuppressive TME. To strengthen this observation, we examined whether RP6530 affected the myeloid-derived suppressor cell (MDSC) compartment *in vivo*. Besides reducing the percentage of tumor-infiltrating and splenic MDSCs (**Fig. 4E**), RP6530 was found to downregulate the expression of iNOS by M-MDSCs, thereby inhibiting their suppressive function in HL tumors (**Fig. 4F**). Furthermore, inhibition of circulating M-MDSCs was correlated with the clinical outcomes of HL patients treated with RP6530 (**Fig. 4G**).

Our current findings demonstrate a PI3Kδ/γ-dependent inhibition of several macrophage-attracting chemokines, such as colony-stimulating factor-1 (CSF-1), CC chemokine ligand 5 (CCL5) and thymus and activation-regulated chemokine (TARC/CCL17) (**Supplementary Fig. S3**). TARC is highly expressed by HRS cells (33), suggesting its role as a biomarker for response evaluation (34). We therefore investigated whether serum TARC levels were correlated with the clinical outcomes of HL patients enrolled in a phase 1 trial (*clinicaltrials.gov identifier NCT02017613*) using RP6530 (35). Upon RP6530 treatment, serum TARC levels were evaluated in 14 HL patients. Patients achieving complete or or partial remission (n= 4) experienced an average mean reduction in serum TARC levels of 40% (range, 4–76%) after 1 month of therapy, whereas the levels were unchanged in patients experiencing SD (n= 7) or PD (n= 3), suggesting that the ability of RP6530 to reduce TARC is likely a result of HL tumor cell death and TAMs repolarization to an M1-like phenotype (**Fig. 4H-I**).

RP6530 reduces tumor angiogenesis and TAM expression of proangiogenic factors. In addition to being immunosuppressive, pro-tumor TAMs contribute to abnormal tumor vasculature (15, 36). Re-polarization of the TAMs phenotype toward M1 by PI3Kδ/γ inhibition was associated with a marked reduction of pro-angiogenic factors (EGF, VEGFA, HIF-1α) (**Fig. 5A**). Given the notion that VEGF is a primary activating factor of angiogenesis and a macrophage chemotactic protein (37, 38), we showed that RP6530 treatment almost completely decreased the expression of VEGF in L-540 and KM-H2 tumors (**Fig. 5B**). Additionally, micro vessel density (average 80% inhibition of endothelial areas, $P < 0.0001$) (**Fig. 5C**), as well as endothelial and tumor Akt and ERK1/2 phosphorylation (**Fig. 5D**) were

411 reduced in RP6530-treated mice. In line with the strong inhibition of ERK1/2 and/or Akt
412 phosphorylation on vascular cells, we detected a severe increase in tumor endothelial cell
413 apoptosis manifested by increased expression of caspase-3 (**Supplementary Fig. S10**).
414
415 **RP6530 suppresses tumor growth in an HL xenograft model and exerts *in vivo* anti-**
416 **proliferative, apoptotic and necrotic effects.** The effect of RP6530 on HL tumor growth was
417 determined. RP6530 significantly ($P < 0.0001$) reduced the *in vivo* growth of L-540 and KM-
418 H2 xenografts [tumor growth inhibition (TGI) = 52% and 46% at 150 mg kg^{-1}, respectively]
419 (**Fig. 6A-B**). These findings were associated with a strong decrease in Ki-67 expression in
420 tumor cells (**Fig. 6C**), suggesting that RP6530 inhibits tumor cell proliferation. Additionally,
421 the anti-proliferative effect was associated with 12-fold increase in tumor cell apoptosis in
422 the KM-H2 nodules, compared with that in the vehicle-treated controls (**Fig. 6D**), suggesting
423 that the effect of RP6530 on tumor cell growth is both cytostatic and cytotoxic. Since
424 apoptosis was a prominent feature of tumor or endothelial cells in RP6530-treated mice,
425 tumors from these animals even showed large areas of non-hemorrhagic tumor necrosis by
426 hematoxylin/eosin as well as TUNEL staining (**Fig. 6E**), suggesting that hypoxic conditions
427 after tumor vessel inhibition might have triggered tumor destruction. RP6530 significantly
428 increased necrotic areas in mice bearing L-540 (3% vs 20%, $P < 0.01$) and KM-H2 (4% vs 26%,
429 $P < 0.0001$) xenografts compared with those in the vehicle-treated controls (**Fig. 6E**).

Discussion

In this study, we demonstrate that the dual PI3Kδ/γ inhibitor RP6530 directly targets HL tumor cells and acts as a critical regulator of signals involved in communication between tumor cells and macrophages. Our data show that PI3Kδ and PI3Kγ are expressed in HL tumor and microenvironmental cells and that inhibition of these isoforms not only suppresses tumor growth and tumor vasculature but also repolarizes tumor-promoting M2-like TAMs toward tumor-suppressive M1-like TAMs by downregulating the limiting glycolytic enzyme pyruvate kinase M2 (PKM2) (39).

Over the past decade, new biological insights have revealed the key role of the TME in the pathogenesis of HL (19). The cross-talk between HRS cells and the cells of the HL microenvironment sustains tumor growth and survival (40). TAMs and MDSCs release immune-suppressive factors that inhibit T-cell-mediated antitumor responses (41), and therapeutic approaches that alter the HL microenvironment, changing it from protective to cytotoxic, hold some promise as novel therapeutics for HL patients (42). Additionally, genomic advances in HL have provided insights into deregulation of key nodal signaling pathways, including the PI3K, NF-kB, and JAK/STAT pathways, which are amenable to small-molecule targeting (43). Among these pathways, the PI3K/Akt pathway and its downstream targets have emerged as central regulators of M2 phenotype activation in macrophages (29). In this context, we considered the high therapeutic potential of targeting the PI3K/Akt pathway to kill HL tumor cells and circumvent the supportive HL microenvironment.

Recent studies have revealed that PKM2-dependent lactic acid production by tumor cells has an important role in the Warburg effect (44). We found that RP6530 inhibits PKM2 in HL cells, preventing its function in regulating the M2-like macrophage polarization through lactate production. Indeed, RP6530 indirectly downregulated the expression of M2 markers in macrophages via HL cells, thus identifying the therapeutic value of reprogramming macrophages in HL. In addition, using specific PKM2 siRNAs, we showed that inhibition of PKM2 is critical for lactate production in HL cells and for stabilization of the M2 phenotype in macrophages; these findings agree with previous studies demonstrating that the activation of PKM2 attenuates the LPS-induced pro-inflammatory M1 macrophage phenotype while promoting traits typical of an M2 macrophage (45). The effects on lactate

production by tumor cells and on cytokines secretion by macrophages were early events detected at 24 h of co-culture and were not influenced by RP6530-induced apoptosis of HL cell lines, an event appearing only after 48 h of RP6530 exposure (**Fig. 1F and Supplementary Fig. S6B**). Additionally, RNA-Seq identified downregulation of PKM2 as a key player in the modulation of macrophages occurring at 6 h of incubation.

Clinical evidences have shown that an increased number of M2-like TAMs is correlated with treatment failure and poor prognosis in HL (21, 22). Therefore, TAM-targeting immunotherapies represent a promising cancer therapeutic approach (41). In addition to preferentially inducing apoptosis in M2-like macrophages, RP6530 inhibits the expression of several macrophage-attracting chemokines, such as CSF-1, CCL5 and TARC/CCL17 in HL cell lines. These *in vitro* findings were further validated by *in vivo* experiments in human tumor xenografts showing that RP6530 not only exerted potent antitumor effects as shown by significant tumor growth inhibition, but also reprogrammed TAMs to an M1-like phenotype. RP6530 directly downregulated the immune-suppressive transcriptional signature of tumor-derived macrophages, thus suppressing the expression of Arg1, TGFβ, and IL10 and stimulating the expression of IL1β and CXCL11. Moreover, RP6530 reduced the percentage of tumor-infiltrating and splenic MDSCs in HL xenografts. Our system using HL cell lines, which are by their very nature microenvironment-independent, represents clearly a limitation to investigate the interaction between the TME and tumor cells. However, the effects that we observed on macrophage reprogramming *in vitro* and the reduction of MDSCs in mice by RP6530, have been validated in a phase 1 trial using RP6530. In this trial, responsive HL patients experienced significant reduction of circulating TARC levels and inhibition of circulating MDSCs. TARC has been implicated in the recruitment of Th2 lymphocytes (46), and in the suppression of classically activated M1 macrophages (47). Reductions in TARC levels were observed in HL patients under standard chemotherapy (33), as well as in HL patients treated with Akt and multikinase inhibitors, supporting its role as a biomarker for response evaluation (34).

Notably, recent data in solid tumors show that PI3Kγ signaling regulates the switch between macrophage polarization and that selectively targeting the γ isoform of PI3K in TAMs inhibited their immunosuppressive phenotype resulting in tumor regression (16, 17). Our

previous finding on the anti-lymphoma efficacy of the PI3Kδ inhibitor TGR-1202 also highlighted the potential of targeting the δ isoform of PI3K in HL (13). Thus, our current work confirmed and expanded these observations by using a dual PI3Kδ/γ inhibitor. Additionally, we demonstrated the effects of PI3Kδ/γ inhibition on tumor vasculature and identified TARC as a potential biomarker of response in HL patients receiving PI3Kδ/γ inhibitor. These findings are particularly relevant to HL patients as the survival, proliferation and immune escape of malignant HRS cells are highly dependent on the interactions with immune microenvironment.

Macrophage recruitment and reprogramming by tumor cells are well known to produce several angiogenic factors that mediate tumor angiogenesis (37). In addition to its critical role in tumor cell survival and cellular metabolism, the PI3K pathway is also involved in angiogenesis (32). Thus, we speculate that targeting PI3Kδ/γ as a common regulator of angiogenesis in macrophages and of tumor cell survival will likely provide a more effective strategy for HL treatment. RP6530 downregulated VEGF expression in tumor cells and TAMs, which led to tumor angiogenesis inhibition and tumor growth reduction. Thus, these findings demonstrated that RP6530 has antiangiogenic effects in HL.

In conclusion, our findings reveal the important signaling role of PI3Kδ/γ in the induction of TAMs polarization and the subsequent promotion of tumor growth in HL. We show that modulating the suppressive phenotype of these cells towards a more inflammatory one can be achieved by targeting PI3Kδ/γ with RP6530. As a consequence, HL tumor burden and tumor vasculature were effectively reduced. Our data establish the first evidence of the translational potential of PI3Kδ/γ inhibition in targeting malignant cells and reshaping the TME in HL.

519 **Author's Contributions**

520 **Conception and design:** S.L.L. and C.C.-S.

521 **Development of methodology:** S.L.L., G.C.

522 **Acquisition of data (provided animals, acquired and managed patients, provided facilities,**
523 **etc.):** S.L.L., G.C., F.M.C., A.M.

524 **Analysis and interpretation of data (e.g., statistical analysis, biostatistics, computational**
525 **analysis):** S.L.L., S.S, C.C.-S.

526 **Writing, review, and/or revision of the manuscript:** S.L.L., C.C.-S., S. Viswanadha, S.
527 Vakkalanka, L.C., A. Santoro, P.A., A. Sica.

528 **Administrative, technical, or material support (i.e., reporting or organizing data,**
529 **constructing databases):** S.L.L., S.S.

530 **Study supervision:** S.L.L. and C.C.-S.

531

532 **Acknowledgements:** Authors thank Alberto Mantovani (Humanitas University, Rozzano,
533 Milan, Italy), and Giorgio Inghirami (Department of Pathology and Laboratory Medicine,
534 Weill Cornell Medical College, Cornell University, New York, USA) for review of the
535 manuscript and discussion.

536

537 **Note:** Supplementary data for this article are available at Clinical Cancer Research Online
538 (http://clincancerres.aacrjournals.org/).

REFERENCES

1. Engert A, Diehl V, Franklin J, Lohri A, Dorken B, Ludwig WD, et al. Escalated-dose BEACOPP in the treatment of patients with advanced-stage Hodgkin's lymphoma: 10 years of follow-up of the GHSG HD9 study. J Clin Oncol. 2009 Sep 20;27(27):4548-54.
2. Canellos GP, Rosenberg SA, Friedberg JW, Lister TA, Devita VT. Treatment of Hodgkin lymphoma: a 50-year perspective. J Clin Oncol. 2014 Jan 20;32(3):163-8.
3. Moskowitz AJ, Perales MA, Kewalramani T, Yahalom J, Castro-Malaspina H, Zhang Z, et al. Outcomes for patients who fail high dose chemoradiotherapy and autologous stem cell rescue for relapsed and primary refractory Hodgkin lymphoma. Br J Haematol. 2009 Jul;146(2):158-63.
4. Younes A. Beyond chemotherapy: new agents for targeted treatment of lymphoma. Nature reviews Clinical oncology. 2011 Feb;8(2):85-96.
5. Younes A, Bartlett NL, Leonard JP, Kennedy DA, Lynch CM, Sievers EL, et al. Brentuximab vedotin (SGN-35) for relapsed CD30-positive lymphomas. N Engl J Med. 2010 Nov 4;363(19):1812-21.
6. Younes A, Gopal AK, Smith SE, Ansell SM, Rosenblatt JD, Savage KJ, et al. Results of a pivotal phase II study of brentuximab vedotin for patients with relapsed or refractory Hodgkin's lymphoma. J Clin Oncol. 2012 Jun 20;30(18):2183-9.
7. Ansell SM, Lesokhin AM, Borrello I, Halwani A, Scott EC, Gutierrez M, et al. PD-1 blockade with nivolumab in relapsed or refractory Hodgkin's lymphoma. N Engl J Med. 2015 Jan 22;372(4):311-9.
8. Carbone A, Gloghini A, Castagna L, Santoro A, Carlo-Stella C. Primary refractory and early-relapsed Hodgkin's lymphoma: strategies for therapeutic targeting based on the tumour microenvironment. J Pathol. 2015 May 7.
9. Kuppers R, Engert A, Hansmann ML. Hodgkin lymphoma. J Clin Invest. 2012 Oct;122(10):3439-47.
10. Fruman DA, Rommel C. PI3Kdelta inhibitors in cancer: rationale and serendipity merge in the clinic. Cancer discovery. 2011 Dec;1(7):562-72.
11. Gopal AK, Kahl BS, de Vos S, Wagner-Johnston ND, Schuster SJ, Jurczak WJ, et al. PI3Kdelta inhibition by idelalisib in patients with relapsed indolent lymphoma. N Engl J Med. 2014 Mar 13;370(11):1008-18.

12. Brown JR, Byrd JC, Coutre SE, Benson DM, Flinn IW, Wagner-Johnston ND, et al. Idelalisib, an inhibitor of phosphatidylinositol 3-kinase p110delta, for relapsed/refractory chronic lymphocytic leukemia. Blood. 2014 May 29;123(22):3390-7.
13. Locatelli SL, Careddu G, Inghirami G, Castagna L, Sportelli P, Santoro A, et al. The novel PI3K-delta inhibitor TGR-1202 enhances Brentuximab Vedotin-induced Hodgkin lymphoma cell death via mitotic arrest. Leukemia. 2016 Sep 2.
14. Rommel C, Camps M, Ji H. PI3K delta and PI3K gamma: partners in crime in inflammation in rheumatoid arthritis and beyond? Nat Rev Immunol. 2007 Mar;7(3):191-201.
15. Hanahan D, Weinberg RA. Hallmarks of cancer: the next generation. Cell. 2011 Mar 4;144(5):646-74.
16. Kaneda MM, Messer KS, Ralainirina N, Li H, Leem CJ, Gorjestani S, et al. PI3Kgamma is a molecular switch that controls immune suppression. Nature. 2016 Nov 17;539(7629):437-42.
17. De Henau O, Rausch M, Winkler D, Campesato LF, Liu C, Cymerman DH, et al. Overcoming resistance to checkpoint blockade therapy by targeting PI3Kgamma in myeloid cells. Nature. 2016 Nov 17;539(7629):443-7.
18. Kaneda MM, Cappello P, Nguyen AV, Ralainirina N, Hardamon CR, Foubert P, et al. Macrophage PI3Kgamma Drives Pancreatic Ductal Adenocarcinoma Progression. Cancer discovery. 2016 Aug;6(8):870-85.
19. Steidl C, Connors JM, Gascoyne RD. Molecular pathogenesis of Hodgkin's lymphoma: increasing evidence of the importance of the microenvironment. J Clin Oncol. 2011 May 10;29(14):1812-26.
20. Liu WR, Shipp MA. Signaling pathways and immune evasion mechanisms in classical Hodgkin lymphoma. Blood. 2017 Nov 23;130(21):2265-70.
21. Steidl C, Lee T, Shah SP, Farinha P, Han G, Nayar T, et al. Tumor-associated macrophages and survival in classic Hodgkin's lymphoma. N Engl J Med. 2010 Mar 11;362(10):875-85.
22. Tan KL, Scott DW, Hong F, Kahl BS, Fisher RI, Bartlett NL, et al. Tumor-associated macrophages predict inferior outcomes in classic Hodgkin lymphoma: a correlative study from the E2496 Intergroup trial. Blood. 2012 Oct 18;120(16):3280-7.

603 23. Koh YW, Park CS, Yoon DH, Suh C, Huh J. CD163 expression was associated with
604 angiogenesis and shortened survival in patients with uniformly treated classical
605 Hodgkin lymphoma. PLoS One. 2014;9(1):e87066.
606 24. Locatelli SL, Careddu G, Stirparo GG, Castagna L, Santoro A, Carlo-Stella C. Dual
607 PI3K/ERK inhibition induces necroptotic cell death of Hodgkin Lymphoma cells through
608 IER3 downregulation. Sci Rep. 2016 Oct 21;6:35745.
609 25. Vakkalanka S, Nyayapathy S, Viswanadha S. RP6530, a dual PI3K delta/gamma
610 inhibitor, potentiates ruxolitinib activity in the JAK2-V617F mutant erythroleukemia
611 cell lines. Cancer Research. 2015 Aug 1;75.
612 26. Lavazza C, Carlo-Stella C, Giacomini A, Cleris L, Righi M, Sia D, et al. Human CD34+ cells
613 engineered to express membrane-bound tumor necrosis factor-related apoptosis-
614 inducing ligand target both tumor cells and tumor vasculature. Blood. 2010 Mar
615 18;115(11):2231-40.
616 27. Alves-Filho JC, Palsson-McDermott EM. Pyruvate Kinase M2: A Potential Target for
617 Regulating Inflammation. Front Immunol. 2016;7:145.
618 28. Colegio OR, Chu NQ, Szabo AL, Chu T, Rhebergen AM, Jairam V, et al. Functional
619 polarization of tumour-associated macrophages by tumour-derived lactic acid. Nature.
620 2014 Sep 25;513(7519):559-63.
621 29. Vergadi E, Ieronymaki E, Lyroni K, Vaporidi K, Tsatsanis C. Akt Signaling Pathway in
622 Macrophage Activation and M1/M2 Polarization. J Immunol. 2017 Feb
623 01;198(3):1006-14.
624 30. Covarrubias AJ, Aksoylar HI, Horng T. Control of macrophage metabolism and
625 activation by mTOR and Akt signaling. Semin Immunol. 2015 Aug;27(4):286-96.
626 31. Sica A, Mantovani A. Macrophage plasticity and polarization: in vivo veritas. The
627 Journal of clinical investigation. 2012 Mar;122(3):787-95.
628 32. Okkenhaug K, Graupera M, Vanhaesebroeck B. Targeting PI3K in Cancer: Impact on
629 Tumor Cells, Their Protective Stroma, Angiogenesis, and Immunotherapy. Cancer
630 discovery. 2016 Oct;6(10):1090-105.
631 33. Weihrauch MR, Manzke O, Beyer M, Haverkamp H, Diehl V, Bohlen H, et al. Elevated
632 serum levels of CC thymus and activation-related chemokine (TARC) in primary
633 Hodgkin's disease: potential for a prognostic factor. Cancer Res. 2005 Jul
634 1;65(13):5516-9.

635 34. Guidetti A, Carlo-Stella C, Locatelli SL, Malorni W, Mortarini R, Viviani S, et al. Phase II
636 study of perifosine and sorafenib dual-targeted therapy in patients with relapsed or
637 refractory lymphoproliferative diseases. Clin Cancer Res. 2014 Nov 15;20(22):5641-51.
638 35. Carlo-Stella C, Delarue R, Barde PJ, Scarfo L, Kumar U, Viswanadha S, et al. Clinical
639 Activity and Safety of RP6530, a Dual PI3Kδ/γ Inhibitor, in Patients with Advanced
640 Hematologic Malignancies: Final Analysis of a Phase 1 Multicenter Study. Blood.
641 2016;128(22):3011-.
642 36. Joshi S, Singh AR, Zulcic M, Durden DL. A macrophage-dominant PI3K isoform controls
643 hypoxia-induced HIF1alpha and HIF2alpha stability and tumor growth, angiogenesis,
644 and metastasis. Mol Cancer Res. 2014 Oct;12(10):1520-31.
645 37. Murdoch C, Muthana M, Coffelt SB, Lewis CE. The role of myeloid cells in the
646 promotion of tumour angiogenesis. Nat Rev Cancer. 2008 Aug;8(8):618-31.
647 38. Lewis CE, Harney AS, Pollard JW. The Multifaceted Role of Perivascular Macrophages
648 in Tumors. Cancer Cell. 2016 Aug 08;30(2):365.
649 39. Iqbal MA, Gupta V, Gopinath P, Mazurek S, Bamezai RN. Pyruvate kinase M2 and
650 cancer: an updated assessment. FEBS Lett. 2014 Aug 19;588(16):2685-92.
651 40. Aldinucci D, Gloghini A, Pinto A, De Filippi R, Carbone A. The classical Hodgkin's
652 lymphoma microenvironment and its role in promoting tumour growth and immune
653 escape. J Pathol. 2010 Jul;221(3):248-63.
654 41. Mantovani A, Marchesi F, Malesci A, Laghi L, Allavena P. Tumour-associated
655 macrophages as treatment targets in oncology. Nature reviews Clinical oncology. 2017
656 Jul;14(7):399-416.
657 42. Vardhana S, Younes A. The immune microenvironment in Hodgkin lymphoma: T cells,
658 B cells, and immune checkpoints. Haematologica. 2016 Jul;101(7):794-802.
659 43. Kuppers R. The biology of Hodgkin's lymphoma. Nat Rev Cancer. 2009 Jan;9(1):15-27.
660 44. Yang L, Xie M, Yang M, Yu Y, Zhu S, Hou W, et al. PKM2 regulates the Warburg effect
661 and promotes HMGB1 release in sepsis. Nat Commun. 2014 Jul 14;5:4436.
662 45. Palsson-McDermott EM, Curtis AM, Goel G, Lauterbach MA, Sheedy FJ, Gleeson LE, et
663 al. Pyruvate kinase M2 regulates Hif-1alpha activity and IL-1beta induction and is a
664 critical determinant of the warburg effect in LPS-activated macrophages. Cell Metab.
665 2015 Jan 06;21(1):65-80.

666 46. Andrew DP, Ruffing N, Kim CH, Miao W, Heath H, Li Y, et al. C-C chemokine receptor 4
667 expression defines a major subset of circulating nonintestinal memory T cells of both
668 Th1 and Th2 potential. J Immunol. 2001 Jan 1;166(1):103-11.
669 47. Katakura T, Miyazaki M, Kobayashi M, Herndon DN, Suzuki F. CCL17 and IL-10 as
670 effectors that enable alternatively activated macrophages to inhibit the generation of
671 classically activated macrophages. J Immunol. 2004 Feb 01;172(3):1407-13.
672

673 **Figure Legends**
674
675 **Fig. 1. RP6530 reduces HL cell proliferation and increases cell death. A-B,** Immunoblots of
676 L-540, KM-H2 and L-428 cells treated with increasing doses of RP6530 (1.25 - 10 µM) for 2 h.
677 All experiments were performed two or more times. **C,** Cytospin preparation showing pAkt
678 (S473) and pERK1/2 expression in L-540, KM-H2 and L-428 cells treated with RP6530 (10
679 µM) for 30 minutes. Scale bar, 20 µm. **D,** Cell proliferation inhibition by RP6530 (1.25 - 10
680 µM) for 48 and 72 h in HL cells. ****P < 0.0001, ***P < 0.001, **P < 0.01; two-sided ANOVA
681 with Dunnett's post-hoc test. **E,** Cell cycle analysis of RP6530 (5-10 µM)-treated L-540, KM-
682 H2, and L-428 cells or vehicle-treated controls after 48 h. ****P < 0.0001, ***P < 0.001, **P
683 < 0.01, *P < 0.05; two-sided ANOVA with Dunnett's post-hoc test, compared with vehicle-
684 treated cells. All data are shown as mean ± s.e.m. and all experiments were performed
685 three times. **F,** Cell death induction by RP6530 (1.25 - 10 µM) for 24, 48 and 72 h in HL cells.
686 Data are shown as mean ± s.e.m. ****P < 0.0001, ***P < 0.001, **P < 0.01, *P < 0.05; two-
687 sided ANOVA with Dunnett's post-hoc test. **G,** Immunoblots of HL cells treated with RP6530
688 or vehicle-treated controls for 48 h. **H,** HL cells were pre-treated with 50 µM Z-VADfmk for 1
689 hour and then treated with 10 µM RP6530 for 48 h. Cell death was assayed by flow
690 cytometry using Annexin V/PI double staining. SU-DHL-8 cell line exposed to sTRAIL 10
691 ng/ml was used as positive control (Ctrl+) for cell death inhibition after Z-VADfmk
692 treatment. ****P < 0.0001; two-sided ANOVA with Tukey's post-hoc test, in comparison to
693 RP6530 alone. All data are shown as mean ± s.e.m. and all experiments were performed two
694 or more times.
695
696 **Fig. 2. RP6530 inhibits tumor glycolysis and HIF1α pathways. A,** Heatmap of the
697 unsupervised hierarchical clustering of 1303 genes that underwent a change in expression
698 (log2FC) in HL cell lines (left). Pathway analysis for KEGG and PID of 111 continuously
699 downregulated genes in the time course (right). Non-significant outcome was obtained in
700 pathway analysis of the 39 continuously upregulated genes at both 6 and 24 h. **B,** The PPI
701 network was generated using the stringApp Cytoscape plug-in. We show only gene sets
702 involved in the HIF1α TF network and glycolysis/gluconeogenesis, which are labeled with
703 the appropriate pathway term. The center of each circle corresponds to the 6 h time point,
704 and the border corresponds to the 24 h time point. The intensity of the node color is

proportional to the log2FC. Yellow indicates upregulation in RP6530-treated samples, and blue indicates downregulation in RP6530-treated samples. Gray nodes are unmodulated or not significantly modulated (adjusted *P*-value > 0.1) genes. The node size is proportional to the score of betweenness centrality. **C,** Heatmap of the four centrality measures of DEGs sorted by the combination score reflecting their important role in the network.

Fig. 3. RP6530-mediated regulation of macrophage polarization. A, Description of co-culture scheme. Co-culture between M2-polarized macrophages (upper chamber) and RP6530- or PKM2 siRNA-treated HL cell lines (lower chamber) was performed for 24 h and 48 h. **B,** L-Lactate production in HL cell lines (lower chamber) was then measured. **C,** mRNA expression of selected M2 markers in M2-polarized macrophages (upper chamber) was determined by RT-PCR after 48 h. The data were normalized to β-actin expression and are expressed relative to the mean of vehicle-treated M2-polarized macrophage cell populations. ****$P < 0.0001$, ***$P < 0.001$, **$P < 0.01$, and *$P < 0.05$ according to two-sided ANOVA with Tukey's post hoc test. The data are shown as the mean ± SEM, and the experiments were performed three times. **D,** Schematic showing the mode of action of RP6530, which inhibits metabolic reprogramming in HL cells, thereby leading to reduction of the M2-like phenotype in macrophages. **E-F,** Immunoblotting of M1 and M2 macrophages treated with vehicle or RP6530 (10 μM) for the indicated time points. The relative levels of phospho/total Akt, phospho/total STAT1 and phospho/total STAT6 in M1 and M2 macrophages are expressed as the percentage of variation in comparison with vehicle-treated macrophages. All the experiments were performed two or more times. **G,** mRNA expression of selected M1 and M2 markers in RP6530-treated (10 μM for 24 h) M1- and M2-polarized macrophages as determined by RT-PCR. The data were normalized to β-actin expression and are expressed relative to the mean of the vehicle-treated M1- or M2-polarized macrophage cell populations. ****$P < 0.0001$, ***$P < 0.001$, and **$P < 0.01$ according to *t*-test. The data are shown as the mean ± SEM, and the experiments were performed three times.

Fig. 4. RP6530 repolarizes TAMs and reduces MDSCs in HL xenografts. A, Representative images of F4/80 expression in HL tumors to identify TAMs. Scale bar, 20 μm. *n* = 3 biological

replicates; one-sided ANOVA with Tukey's post hoc test. All the data are shown as the mean ± SEM, and all the experiments were performed two times. **B,** Histogram bars show the percentage change in each cell population ($CD45^+$ and TAM) in the RP6530-treated group compared with those in the vehicle-treated controls. **C,** Flow cytometric analysis and quantification of $CD11b^+F4/80^+$ (TAM) cell populations in vehicle- and RP6530-treated L-540 and KM-H2 tumors and expression of CD86 and MHC-II (M1) as well as CD206 and CD301 (M2) in $CD11b^+F4/80^+$ cell populations. *n* = 3 biological replicates; ***$P < 0.001$, **$P < 0.01$, and *$P < 0.05$ according to *t*-test. All the data are shown as the mean ± SEM, and all the experiments were performed two times. **D,** mRNA expression of selected M1 and M2 markers in the vehicle- and RP6530-treated L-540- and KM-H2-derived TAMs as determined by RT-PCR. *n* = 3 biological replicates. The data were normalized to β-actin expression and are expressed relative to the mean of vehicle-treated tumors. All the data are shown as the mean ± SEM, and all the experiments were performed two times. **E-F,** Flow cytometric analysis and quantification of tumor and splenic M-MDSC cell population in vehicle and RP6530-treated L-540 tumors; expression of $CD11b^+Ly6C^{high}$ (M-MDSC), $CD11b^+Ly6G^+$ (G-MDSC) in $CD45^+$ cell population and iNOS in M-MDSC. Mean fluorescence intensity (MFI). *n* = 5 biological replicates; ***$P < 0.001$, **$P < 0.01$; *t*-test. All data are shown as mean ± s.e.m. and all experiments were performed two times. **G,** Fold change over baseline (BL) of the percentage of M-MDSC in PBLs after 1 month (C2D1), 2 months (C3D1) and 3 months (C4D1) of RP6530 administration in HL patients. Human M-MDSC were identified within the gate of $HLA\text{-}DR^{low\text{-}neg}$ cells as $CD33^{high}CD14^+$ cells. Data are represented as box plots displaying the median, 25th and 75th percentiles as boxes and the 10th and 90th percentiles as whiskers. CR = Complete Response and PR = Partial Response (n= 4); SD = Stable Disease (n= 7); PD = Progressive Disease (n=5). **H,** Percentage of variations over baseline of TARC levels (pg/ml) in HL patient sera after 1 to 12 months (C2D1 to C14D1) of RP6530 administration. **I,** Fold change (FC) over baseline (BL) of TARC levels (pg/ml) in HL patient sera after 1 month (C2D1) of RP6530 administration. CR = Complete Response and PR = Partial Response (n= 4); SD = Stable Disease (n= 7); PD = Progressive Disease (n=3).

Fig. 5. RP6530 inhibits tumor vasculature in HL xenografts. A, mRNA expression of selected angiogenesis markers in the vehicle- and RP6530-treated L-540-derived TAMs as

767 determined by RT-PCR. *n* = 3 biological replicates. The data were normalized to β-actin
768 expression and are expressed relative to the mean of the vehicle-treated tumors. All the
769 data are shown as the mean ± SEM, and all the experiments were performed two times. **B,**
770 Representative histological images of VEGFA staining of the vehicle- and RP6530-treated L-
771 540 and KM-H2 tumors. Scale bar, 20 µm. **C,** Representative histological images and
772 quantification of tumor vasculature (streptavidin staining) in the vehicle- and RP6530-
773 treated HL tumors. Scale bar, 20 µm. *n* = 3 biological replicates; **P* < 0.001 according to *t*-
774 test. **D,** Immunofluorescence analysis of pAkt and pERK1/2 in the vehicle- and RP6530-
775 treated L-540 and KM-H2 tumors. Arrows and arrowheads indicate pAkt and pERK1/2
776 expression in endothelial cells and tumor cells, respectively. Scale bar, 50 µm. **E,** Model
777 depicting the effect of RP6530 on HL tumor cells and the HL TME. RP6530 converts TAMs
778 into pro-inflammatory macrophages, leading to the inhibition of tumor vasculature and the
779 suppression of tumor growth.
780
781 **Fig. 6. RP6530 reduces tumor growth and increases tumor necrosis. A,** Therapy regimen
782 (top panel; PO, *per os*; WK, week; BID, twice a day) and the mean ± SEM tumor volume of
783 subcutaneous L-540 and KM-H2 implants in the mice treated with the vehicle or RP6530
784 (100 and 150 mg kg^{-1} administered orally twice a day; bottom panel). *n* = 10 mice per group.
785 **P* < 0.0001 according to two-sided ANOVA with Dunnett's post hoc test. **B,** Mean weight (±
786 SEM) values were assessed. **C**-**E,** L-540 and KM-H2 tumors treated with RP6530 (150 mg kg^{-1}
787 twice a day for 5 days) or vehicle control. **C,** Ki-67 expression based on
788 immunohistochemistry of L-540 and KM-H2 tumor sections at day 5 after treatment with
789 RP6530 or vehicle. Scale bar, 100 µm. **D,** Images (left panel) and quantification (right panel)
790 of apoptotic tumor cells detected by TUNEL staining. Scale bar, 1 µm. *n* = 3 mice per group.
791 Each dot represents the value obtained from the analysis of a single tissue field, and the
792 lines indicate the mean ± SEM. **P* < 0.0001 according to *t*-test. **E,** Representative TUNEL and
793 hematoxylin and eosin-stained sections (H&E) of L-540 and KM-H2 tumors at day 5 after
794 treatment with RP6530 or the vehicle (left panel). Quantification of tumor necrosis (right
795 panel). *n* = 3 mice per group. At least three sections from different animals were analyzed
796 per treatment group. The boxes extend from the 25th to the 75th percentiles, the lines

797 indicate the median values, and the whiskers indicate the range of the values. *P < 0.001
798 and *P < 0.0001 according to t-test. All the experiments were performed two or more times.

Figure 1

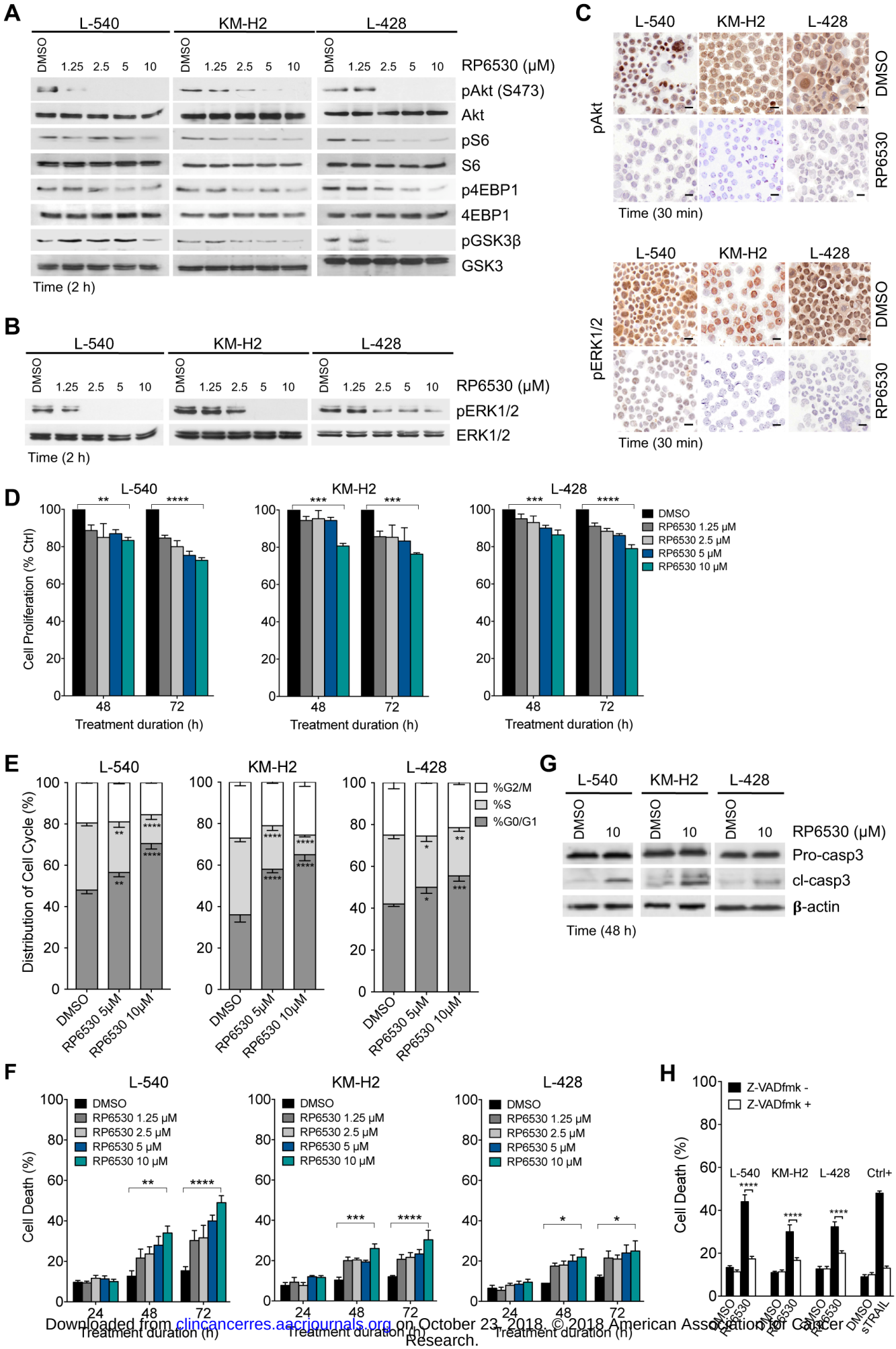

Figure 2

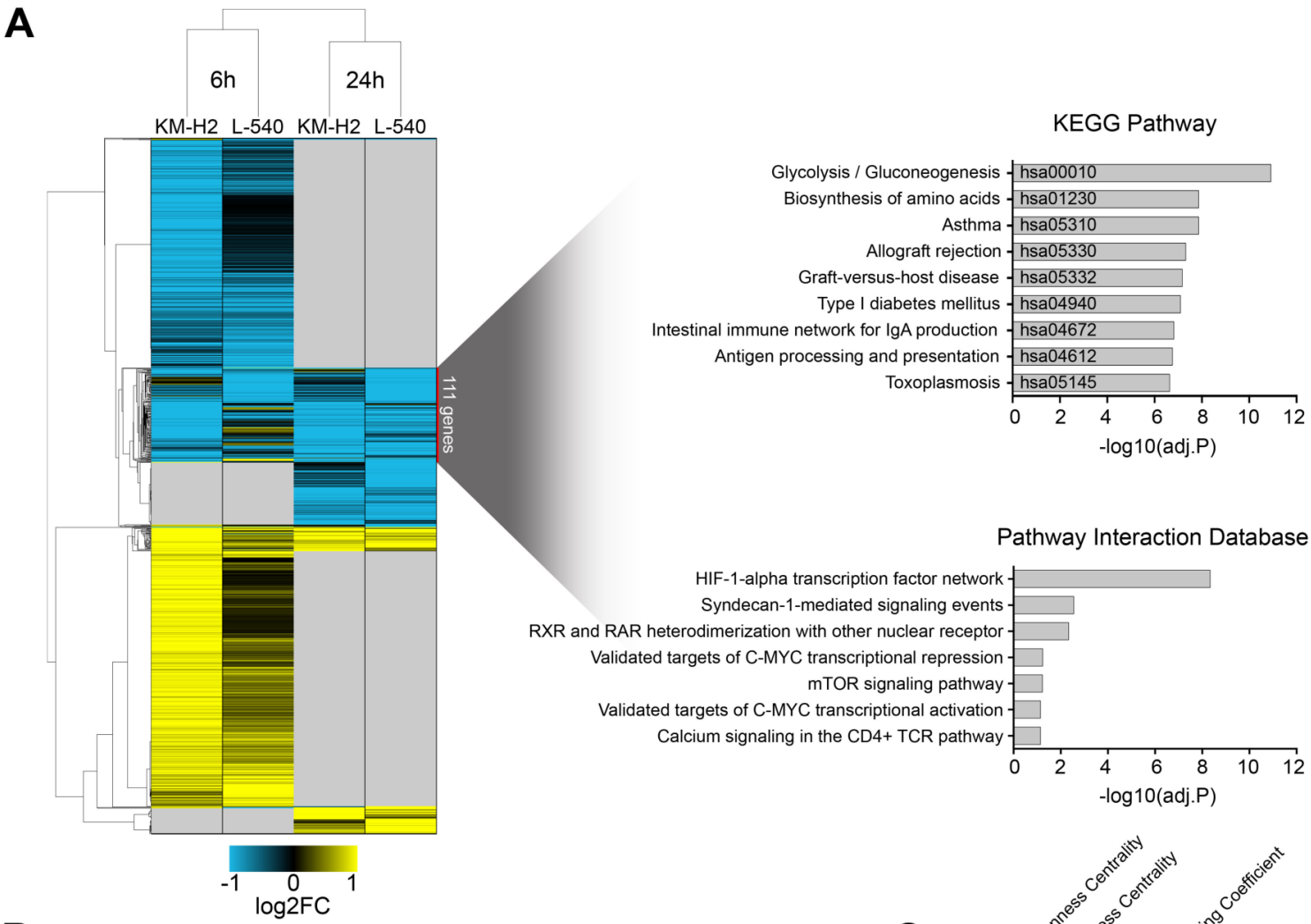

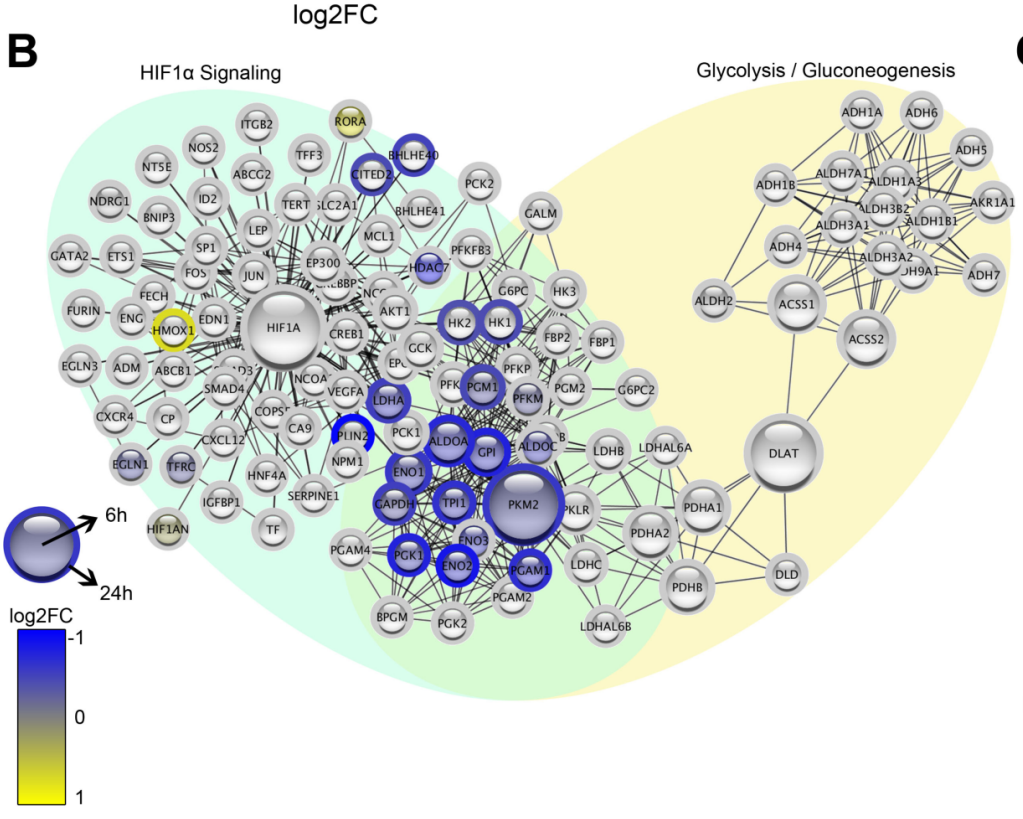

Figure 3

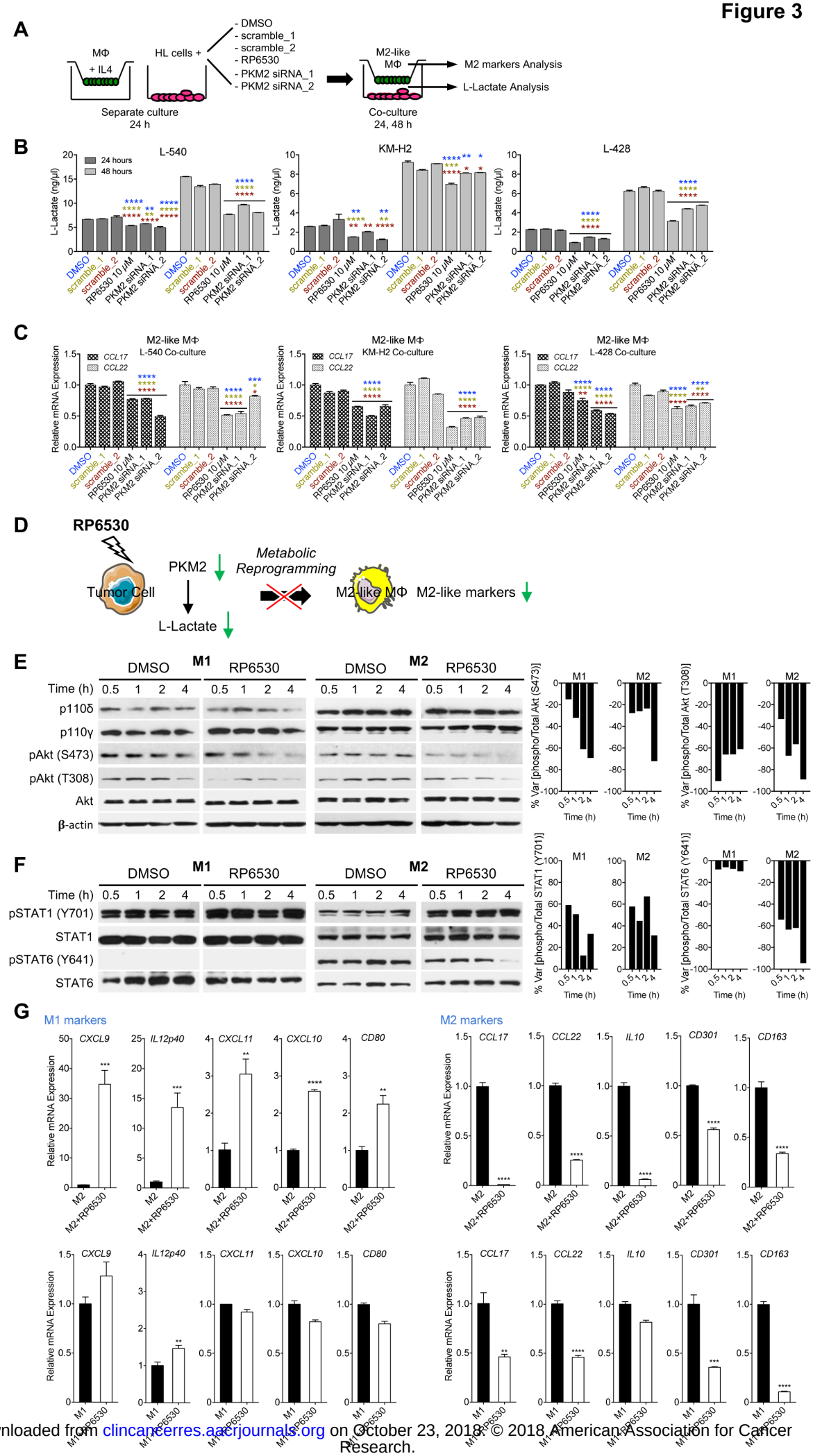

Figure 4

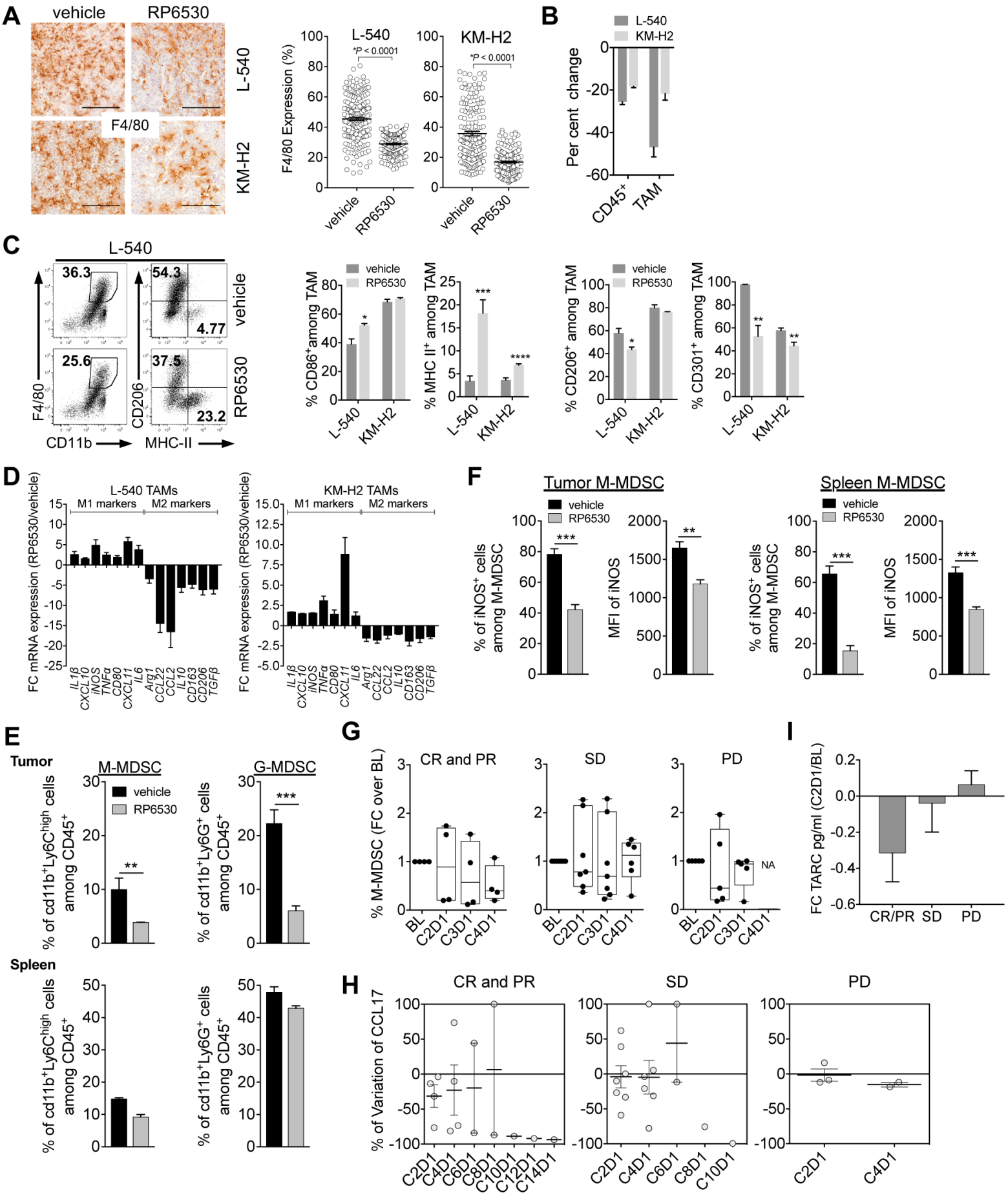

Figure 5

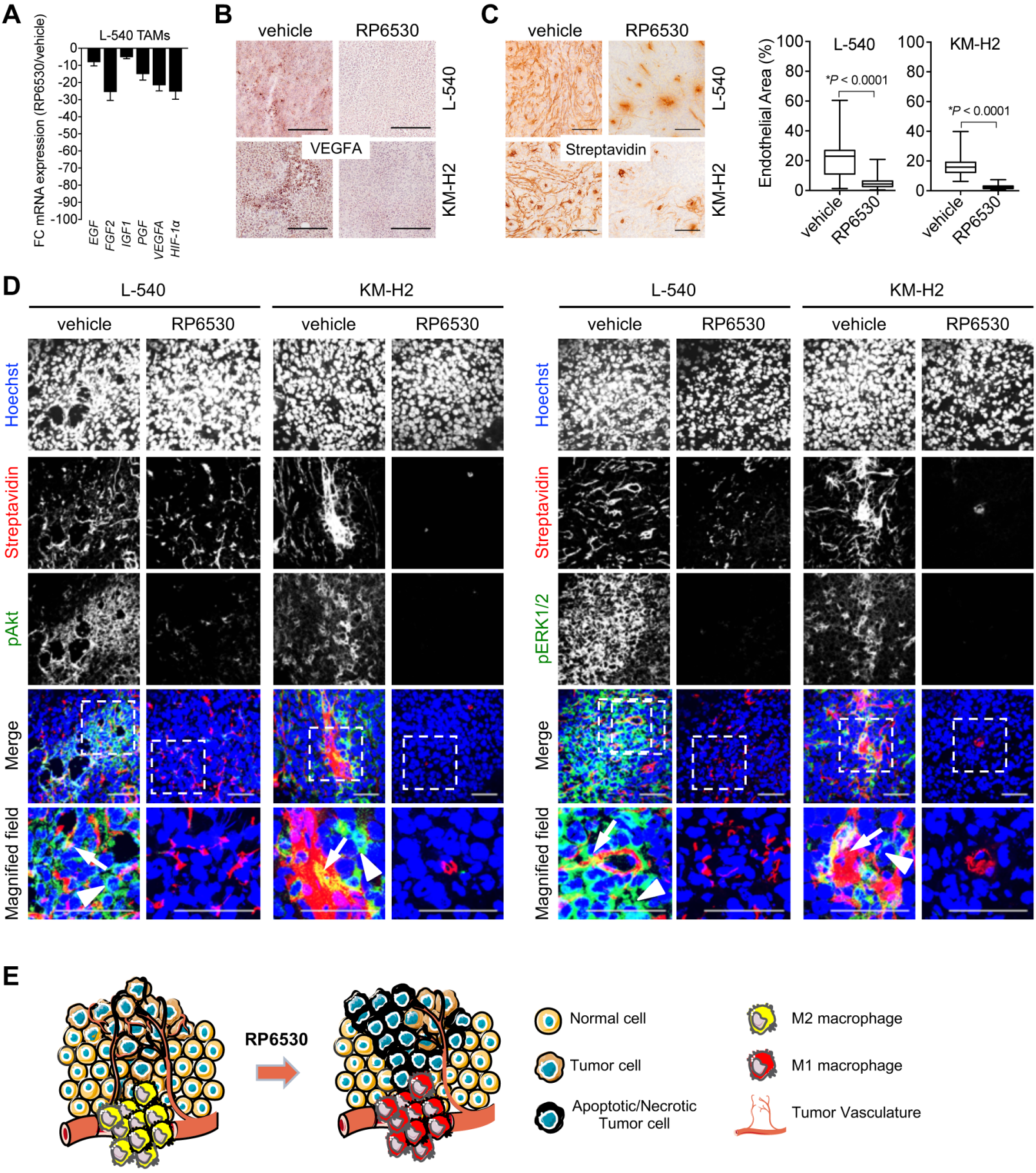

Figure 6

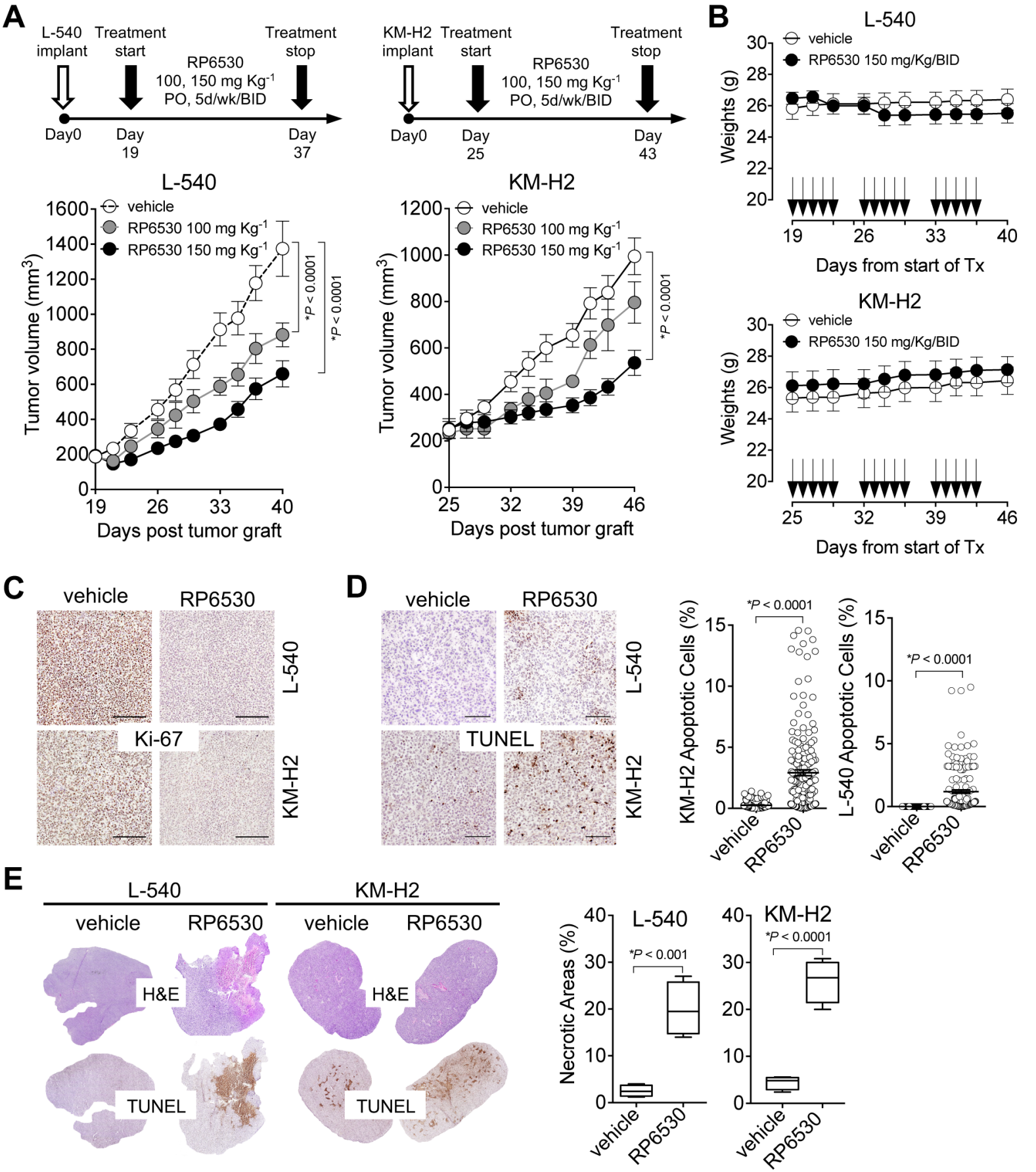

AACR American Association for Cancer Research

Clinical Cancer Research

Targeting cancer cells and tumor microenvironment in preclinical and clinical models of Hodgkin lymphoma using the dual PI3Kδ/γ inhibitor RP6530

Silvia Laura Locatelli, Giuseppa Careddu, Simone Serio, et al.

Clin Cancer Res Published OnlineFirst October 23, 2018.